# Tensor-product state approach to spin-$\frac{1}{2}$ square $J_1$-$J_2$ antiferromagnetic Heisenberg model: Evidence for deconfined quantum criticality

Ling Wang,[1,2] Zheng-Cheng Gu,[3,4] Frank Verstraete,[5,6] and Xiao-Gang Wen[7,4]

[1]*Beijing Computational Science Research Center, 10 West Dongbeiwang Road, Beijing 100193, China*

[2]*Institute of Quantum Information and Matter and Department of Physics, California Institute of Technology, Pasadena, California 91125, USA*

[3]*Department of Physics, The Chinese University of Hong Kong, Shatin, New Territories, Hong Kong*

[4]*Perimeter Institute for Theoretical Physics, Waterloo, Ontario, Canada N2L 2Y5*

[5]*Vienna Center for Quantum Science and Technology, Faculty of Physics, University of Vienna, Boltzmanngasse 5, A-1090 Vienna, Austria*

[6]*Department of Physics and Astronomy, Ghent University, Krijgslaan 281-S9, B-9000 Gent, Belgium*

[7]*Department of Physics, Massachusetts Institute of Technology, Cambridge, Massachusetts 02139, USA*

(Received 24 May 2016; published 19 August 2016)

The ground state phase of a spin-$\frac{1}{2}$ $J_1$-$J_2$ antiferromagnetic Heisenberg model on a square lattice around the maximally frustrated regime ($J_2 \sim 0.5J_1$) has been debated for decades. Here we study this model using the cluster update algorithm for tensor-product states (TPSs). The ground state energies at finite sizes and in the thermodynamic limit (with finite size scaling) are in good agreement with exact diagonalization study. Through finite size scaling of the spin correlation function, we find the critical point $J_2^{c1} = 0.572(5)J_1$ and critical exponents $\nu = 0.50(8)$, $\eta_s = 0.28(6)$. In the range of $0.572 < J_2/J_1 \leqslant 0.6$ we find a paramagnetic ground state with an exponentially decaying spin-spin correlation. Up to a $24\times24$ system size, we observe power law decaying dimer-dimer and plaquette-plaquette correlations with an anomalous plaquette scaling exponent $\eta_p = 0.24(1)$ and an anomalous columnar scaling exponent $\eta_c = 0.28(1)$ at $J_2/J_1 = 0.6$. These results are consistent with a potential gapless $U(1)$ spin-liquid phase. However, since the $U(1)$ spin liquid is unstable due to the instanton effect, a valence bond solid order with very small amplitude might develop in the thermodynamic limit. Thus, our numerical results strongly indicate a deconfined quantum critical point at $J_2^{c1}$. Remarkably, all the observed critical exponents are consistent with the $J$-$Q$ model.

DOI: 10.1103/PhysRevB.94.075143

## I. INTRODUCTION

The spin-$\frac{1}{2}$ $J_1$-$J_2$ antiferromagnetic Heisenberg model on a square lattice has drawn great attention for the last two decades owing to its close relation to the disappearance of antiferromagnetic (AF) long-range order (LRO) in high-$T_c$ superconducting materials [1,2], and has been proposed as a possible simple model to realize a topologically ordered chiral spin-liquid state [3,4] or $Z_2$ spin-liquid state [5–9]. The Hamiltonian of this model is given by

$$H = J_1 \sum_{(i,j)} \mathbf{S_i} \cdot \mathbf{S_j} + J_2 \sum_{\langle i,j \rangle} \mathbf{S_i} \cdot \mathbf{S_j} \quad (J_1, J_2 > 0), \qquad (1)$$

where $(i,j)$ represents the nearest-neighbor (NN) pair and $\langle i,j \rangle$ represents the next-nearest-neighbor (NNN) pair. For convenience, we set $J_1 = 1$ throughout the paper. It has long been believed that the frustration from the NNN interaction competes with the NN one and drives the system through a quantum phase transition from an AF LRO phase to a magnetically disordered phase. In two extreme cases, the ground state phases of the model are well established: At very small $J_2$, the ground state has AF LRO, and at very large $J_2$, the system falls into two weakly coupled sets, and the magnetic susceptibility peaks at momentum $(\pi,0)$ or $(0,\pi)$. In the intermediate coupling regime, quantum fluctuation is meant to destroy the AF LRO near the maximally frustrated point $J_2 = 0.5$ of the classical model and establish a new paramagnetic phase. The nature of such a quantum phase is of great interest.

Numerous efforts have been made using many different approaches, such as the exact diagonalization (ED) [10–15], spin-wave theory [16,17], series expansion [18,19], large-$N$ expansion [5], the coupled cluster method (CCM) [20], variational methods [including short-range resonating valence bond (SRVB) method] [21–23], and the fixed-node quantum Monte Carlo (QMC) [24]. The results turned out to be controversial: A series expansion calculation of a general magnetic susceptibility over different perturbation fields suggests that within the Ginzburg-Landau paradigm the type of phase transition from the Néel to paramagnetic phase is of first order [19]. However, the same general magnetic susceptibility calculated with a coupled cluster method suggests a second-order phase transition [20]. The nature of the phase near $J_2 = 0.5$ was as unclear: A fixed-node QMC study indicates a plaquette valence bond solid (VBS) state [24], whereas the series expansion argues for a columnar VBS state [19]. A relatively direct investigation of the nature of the ground state order is using the SRVB approximation [22], where with another term $J_3$ included in the Hamiltonian, a plaquette VBS state along the line of $J_2 + J_3 = 0.5$ is found. Most recently, the density matrix renormalization group (DMRG) has demonstrated its power in simulating quasi-one-dimensional cylinders for the kagome Heisenberg model. Different groups applied it to the spin-$\frac{1}{2}$ $J_1$-$J_2$ model as well, however, the results were different: Jiang *et al.* claim a $Z_2$ spin-liquid state [25] while Gong *et al.* suggest a plaquette VBS state [26].

In this paper, we revisit this problem with a tensor-product state (TPS) [27] ansatz for the ground state wave function, accessed by the recently proposed cluster update

 

algorithm [28], and reveal the answer to both questions. By fitting a universal scaling function for the spin-spin correlation we observe a continuous phase transition from the Néel to paramagnetic phase at $J_2^{c1} = 0.572(5)$ with critical exponents $\nu = 0.50(8)$ and $\eta_s = 0.28(6)$. In the paramagnetic phase we find exponentially decaying spin-spin correlation functions. Up to a $24\times24$ system size, we observe power law decaying dimer-dimer and plaquette-plaquette correlation functions, which indicate a nonzero spin triplet gap and a zero spin singlet gap. These properties are consistent with the previously proposed $U(1)$ gapless spin-liquid state [29] by using a one-parameter TPS ansatz. Nevertheless, it is well known that the $U(1)$ gapless spin liquid is unstable due to the instanton effect, and we argue that a very small VBS order might eventually develop in the thermodynamic limit. Interestingly, at $J_2 = 0.6$ the scaling of plaquette (columnar) VBS order parameter suggests an anomalous VBS scaling exponent $\eta_p = 0.24(1)$ [$\eta_c = 0.28(1)$]. Remarkably, all observed exponents are consistent with those of the $J$-$Q$ model [30–32]. Thus, our numerical results strongly indicate a deconfined quantum critical point scenario (DQCP) [33,34] from Néel order to VBS order at $J_2 = 0.572(5)$.

## II. RESULTS

We divide the square lattice into four sublattices $A, B, C, D$ that form a $2\times2$ unit cell, and associate each type of site with one of the four different sublattice tensors. Such a choice of tensor-product state ansatz aims at describing potential VBS orders and studying their competing effects. We use the cluster update imaginary time evolution method [28] to evolve from a TPS with random initialized tensor elements to a converged state of the $J_1$-$J_2$ Hamiltonian. Such an obtained state is often called infinite TPS, since there is no system size information entering into this evolution scheme. Once the infinite TPS (with a bond dimension $D = 9$) converges, we cover a $L\times L$ torus with repeated $2\times2$ unit cells and form a finite size wave function. Without further finite size ground state optimization, we measure the size-dependent variational energies, staggered magnetizations, spin-spin, dimer-dimer, and plaquette-plaquette correlations on $L\times L$ tori for $L = 4$, 6, 8, 12, 16, and 24. Our tensor measurement strategy is to use variational Monte Carlo (VMC) [35] to sample spin configurations, whose weights are computed by the tensor renormalization idea [36,37]. With these combined techniques, we can make precise measurements (for periodic systems) and perform a careful finite size scaling analysis. Hereafter, all our numerical results are obtained from TPSs with a bond dimension $D = 9$.

*Ground state energies*. We present the ground state energies on tori of $L\times L$ (at $L = 8$ and 16) as functions of $D_c$ ($D_c = 8$, 10, 12, 16, 20, 24, and 28) in Fig. 1, where $D_c$ is the Schmidt number kept in calculating the importance weight of the sampled spin configurations [35]. We find that the variational ground state energies decrease monotonically with increasing $D_c$. Using a quadratic function in $1/D_c^2$, we extrapolate the finite size energies to the $D_c \to \infty$ limit. The fitted results are shown in the dashed curves in Fig. 1. Note that our measurement scheme [35] makes approximations to the importance weight of the sampled spin configurations, where error is

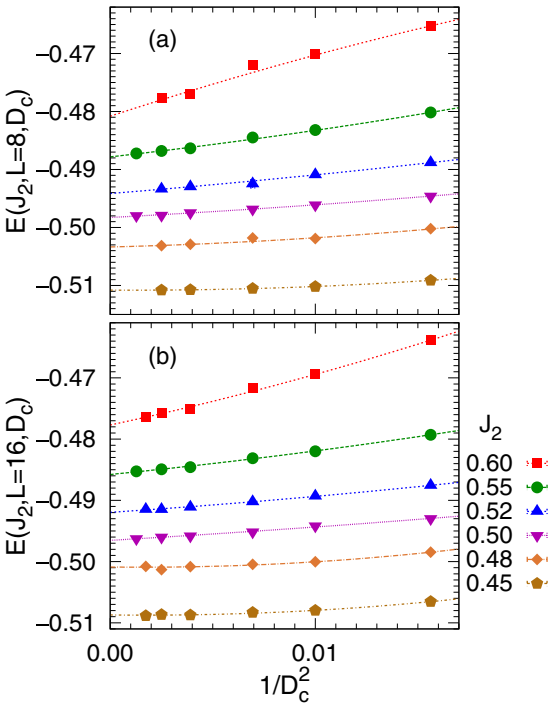


FIG. 1. Finite size ground state energies using the largest available bond dimension $D = 9$ measured at various $D_c = 8$, 10, 12, 16, 20, 24, and 28 in a variational Monte Carlo (VMC)-tensor renormalization algorithm [35]. The finite size energies are extrapolated to $D_c \to \infty$ limit by fitting to second-order polynomials; the fitted results are shown in the dashed lines.

controlled by $D_c$. However, the VMC principle guarantees that all measured energies at finite $D_c$ are variational. Furthermore, the almost-converged energies at $D_c = 28$ make sure that the extrapolations are reliable.

We compare our variational energies on tori with the SU(2) symmetric DMRG results on tori [26] and the best VMC with Lanczos projection steps [9] on tori. As seen in Fig. 2, at a system size $L = 8$, our results are consistent with the DMRG

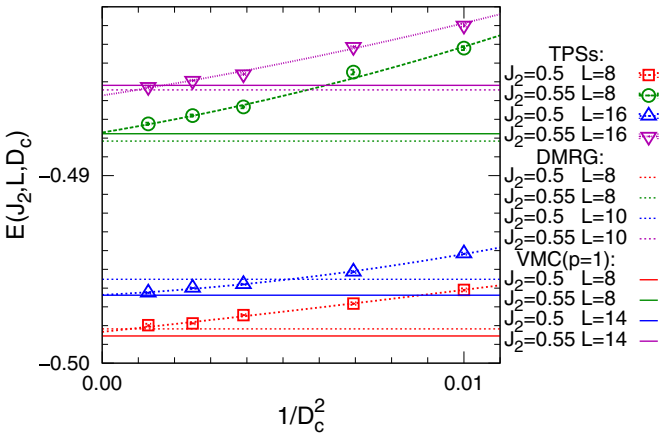


FIG. 2. A benchmark of ground state energy with the SU(2) symmetric DMRG results [26] on tori and the VMC calculation with one Lanczos projection step [9] on tori at $J_2 = 0.5$ and 0.55, where $D_c$ is the Schmidt number kept in our VMC-tensor renormalization algorithm.

results. Interestingly, our variational energies on tori of $L = 16$ are lower than the DMRG energies on tori of $L = 10$. This means that the ground state entanglement on tori of $10\times10$ are beyond the resolution of the DMRG if we keep only 8000 SU(2) Schmidt states, which also explains why DMRG often relies on cylinder studies instead of tori. Very impressively, our variational ground state energy for $L = 16$ is comparable to (at $J_2 = 0.5$) or better than (at $J_2 = 0.55$) the best VMC results for a smaller size $L = 14$ torus with one-step Lanczos projections [9].

*Staggered magnetization*. The staggered magnetization square is defined as

$$M^2 = \frac{1}{N}\sum_{r_x,r_y}(-1)^{r_x+r_y}C(r_x,r_y), \tag{2}$$

where $C(r_x,r_y)$ is the spin-spin correlation function,

$$C(r_x,r_y) = \frac{1}{N}\sum_{x,y}\mathbf{S}_{(x,y)}\cdot\mathbf{S}_{(x+r_x,y+r_y)}. \tag{3}$$

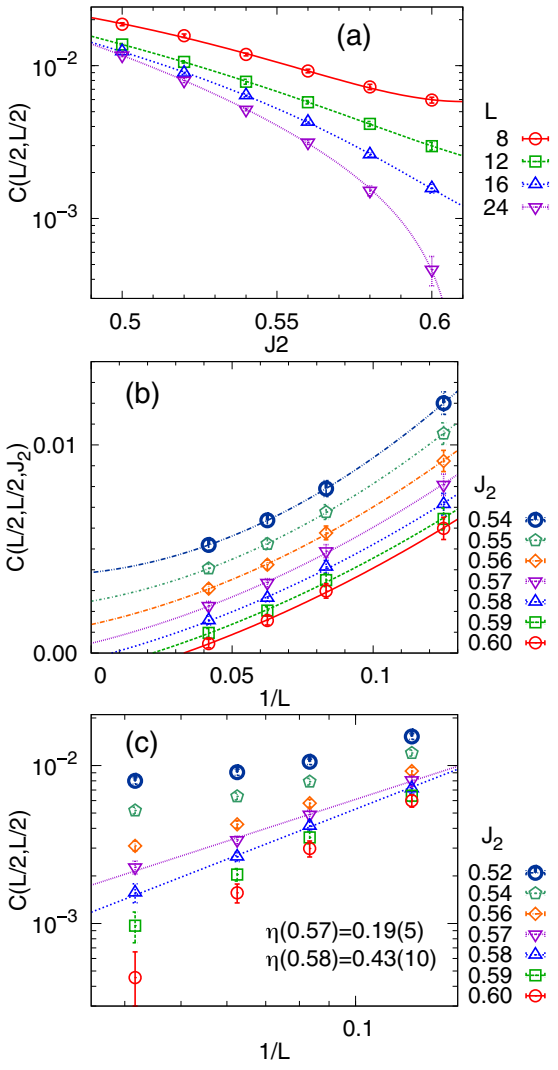


FIG. 3. (a) The largest distance spin-spin correlation as a function of $J_2$ at $L = 8$, 12, 16, 24. The same correlations $C(L/2,L/2)$ presented against $1/L$ in a regular plot (b) and in a log-log plot (c) for various $J_2$.

We compute the spin-spin correlation functions at the largest distance $C(L/2,L/2)$ for various $L$, and show their dependence with coupling $J_2$ in Fig. 3(a), where dashed lines are polynomial fittings. To determine the critical transition point, we present $C(L/2,L/2)$ against $1/L$ in a regular plot for various $J_2$ in Fig. 3(b), and extrapolate using quadratic functions (shown in the dashed lines). We find the critical point to be $0.57 < J_2^{c_1} < 0.58$. To see the critical behavior, we present $C(L/2,L/2)$ vs $1/L$ in a log-log plot in Fig. 3(c). Taking the critical scaling as $C(L/2,L/2) \propto L^{-(z+\eta_s)}$ and using a linear regression function, we find the anomalous spin scaling exponent $\eta_s = 0.19(5)$ at $J_2 = 0.57$ and $\eta_s = 0.43(10)$ at $J_2 = 0.58$. Finally, we take the finite size scaling (FSS) formula

$$\begin{aligned} &C(L/2,L/2)L^{z+\eta_s}(1+aL^{\omega}) \\ &\quad = F\left[\left(J_2^{c_1}-J_2\right)L^{1/\nu}(1+bL^{\omega})\right] \end{aligned} \tag{4}$$

to determine the critical point $J_2^{c_1} = 0.572(5)$ and the critical exponents $\nu = 0.50(8)$, $\eta_s = 0.28(6)$, with the result presented in Fig. 4. Here, $F(x)$ is a dimensionless polynomial, and $\omega$ represents subleading finite size corrections whose values are set to 2.

*Valence bond solid orders*. To determine the phase at region $J_2 \in (0.572,0.6]$, dimer-dimer and plaquette-plaquette correlation functions are investigated. We define the dimer-dimer correlation function as

$$C_{dx}(r_x,r_y) = \frac{1}{N}\sum_{x,y}D_x(x,y)D_x(x+r_x,y+r_y), \tag{5}$$

$$C_{dy}(r_x,r_y) = \frac{1}{N}\sum_{x,y}D_y(x,y)D_y(x+r_x,y+r_y), \tag{6}$$

with

$$D_x(x,y) \equiv \mathbf{S}_{(x,y)}\cdot\mathbf{S}_{(x+1,y)}, \tag{7}$$

$$D_y(x,y) \equiv \mathbf{S}_{(x,y)}\cdot\mathbf{S}_{(x,y+1)}. \tag{8}$$

Similarly, the plaquette correlation function is [22,38]

$$C_{\mathrm{plq}}(r_x,r_y) = \frac{1}{N}\sum_{x,y}Q(x,y)Q(x+r_x,y+r_y), \tag{9}$$

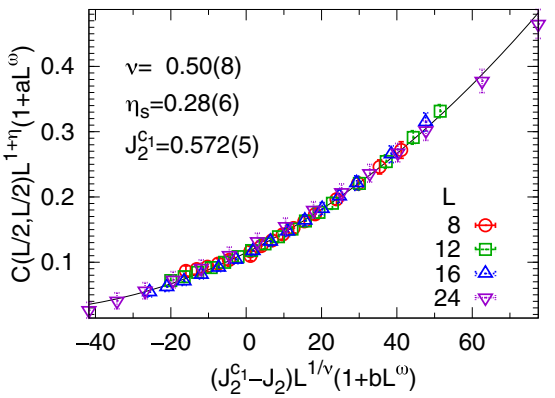


FIG. 4. The finite size scaling function of $C(L/2,L/2)$.

with $Q(x,y) \equiv [P_{\square}(x,y) + P_{\square}^{-1}(x,y)]$ defined as the permutation operator that permutes four spins on a plaquette by one lattice spacing.

To subtract the background expectation value, we take the modified correlation functions as follows:

$$C^*_{dx}(r,r) = C_{dx}(r,r) - C_{dx}(r-1,r-1), \tag{10}$$

$$C^*_{\rm plq}(r,r) = C_{\rm plq}(r,r) - C_{\rm plq}(r-1,r-1). \tag{11}$$

We present the modified dimer-dimer and plaquette-plaquette correlation functions for $J_2 = 0.6$ and $L = 8$, 12, 16, and 24 in Fig. 5. We find clear power law decay behaviors for both the dimer-dimer and plaquette-plaquette correlations. To measure the two most possible VBS orders, namely, the *columnar* VBS order and the *plaquette* VBS order, we define the following order parameters:

$$S^2_{\rm plq}(L) = \frac{1}{L-2}\sum_{r=2}^{L}(-1)^r C_{\rm plq}(r,r), \tag{12}$$

$$S^2_{\rm col}(L) = \frac{1}{L-2}\sum_{r=2}^{L}(-1)^r C_{dx}(r,r). \tag{13}$$

We show the above two VBS order parameters at $J_2 = 0.6$ as a function of $1/L$ in a log-log plot in Fig. 6. Again, we find power law decay behaviors for both the *columnar* and *plaquette* VBS orders. Taking the critical scaling behavior as $S^2_{\rm VBS}(L) \propto L^{-(z+\eta)}$, we find the anomalous plaquette scaling exponent $\eta_p = 0.24(1)$ and the anomalous columnar scaling exponent $\eta_c = 0.28(1)$. Our critical exponents $\eta_s$, $\eta_c$, $\eta_p$, and $\nu$ are all consistent with the results of the $J$-$Q$ model [30–32].

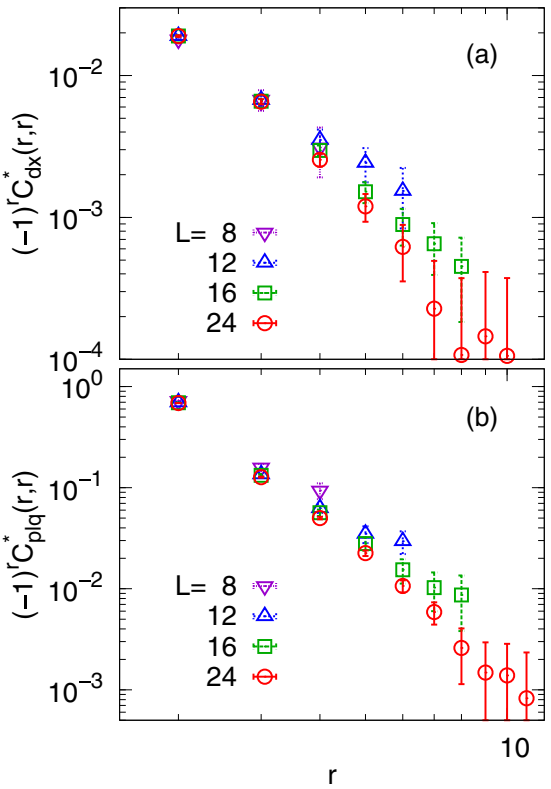


FIG. 5. The modified dimer-dimer correlation $C^*_{dx}(r,r)$ (a) and plaquette-plaquette correlation $C^*_{plq}(r,r)$ (b) as a function of separation $r$ at $J_2 = 0.6$ in log-log plots.

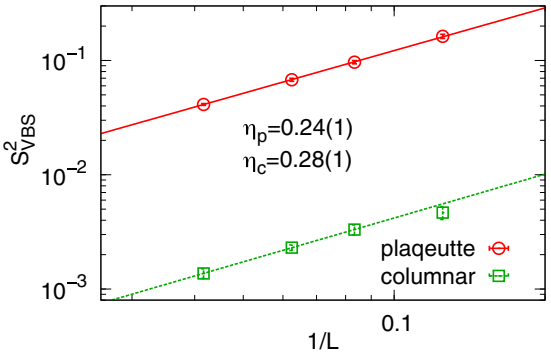


FIG. 6. The valence bond solid order parameters $S^2_{\rm col}$ and $S^2_{\rm plq}$ at $J_2 = 0.6$ as functions of $1/L$ in a log-log plot. The power law decay behaviors are captured by decay exponents $1+\eta_p = 1.24(1)$ and $1+\eta_c = 1.28(1)$ for the plaquette and columnar VBS order, respectively.

*Gapless spin liquid versus deconfined quantum criticality.* The exponentially decaying spin-spin correlation and power law decaying dimer-dimer correlation indicate that the paramagnetic phase has a spin $S = 1$ gap but no $S = 0$ gap. These properties are consistent with the gapless $U(1)$ spin-liquid state constructed by a single variational parameter TPS ansatz [29]. However, since it is well known that a $U(1)$ gapless spin-liquid state is unstable due to the confinement of $U(1)$ gauge field in $2+1$ dimensions, we argue that a VBS order with an exponentially small amplitude might eventually develop at long wavelengths. Thus, our numerical results could imply a Landau forbidden phase transition from Néel order to VBS order described by the DQCP scenario.

## III. CONCLUSIONS

In conclusion, we applied the cluster update algorithm for tensor-product states (TPSs) to study the frustrated spin-$\frac{1}{2}$ $J_1$-$J_2$ antiferromagnetic Heisenberg model on a square lattice. Limited to a cluster size $2\times2$, a rather large bond dimension $D = 9$ is feasible. Through a finite $D_c$ scaling, our ground state energies at finite sizes are in good agreement with the results from a state-of-the-art exact diagonalization (ED) study [15], an SU(2) symmetric density matrix renormalization group (DMRG) study [26], and a variational Monte Carlo (VMC) study [9]. Applying finite size scaling (FSS) to the spin-spin correlation function, we found the staggered magnetization diminishes to zero at $J_2^{c_1} = 0.572(5)$, suggesting a continuous quantum phase transition. We further observed an exponentially decaying spin-spin correlation with power law decaying dimer-dimer and plaquette-plaquette correlations up to a $24\times24$ system size. All this evidence points to the emergence of a gapless $U(1)$ spin-liquid state that is consistent with a single variational parameter TPS ansatz [29]. Nevertheless, since the $U(1)$ spin liquid is unstable due to the instanton effect, a VBS order with a small amplitude could emerge in the thermodynamic limit. Remarkably, we found the critical exponents $\nu = 0.50(8)$ and $\eta_s = 0.28(6)$,

$\eta_p = 0.24(1)$, $\eta_c = 0.28(1)$, which agree with the observed critical exponents for a deconfined quantum critical point (DQCP) in the $J$-$Q$ model on a square lattice [30–32]. Thus our numerical results strongly indicate a Landau forbidden phase transition from Néel order to VBS order at $J_2^{c_1}$.

## IV. METHOD

The following is an illustration of how to construct the evolution operators for this Hamiltonian. We expand the evolution operator $\hat{\mathbf{O}} \sim \exp\{-\epsilon J_1(\mathbf{S}_1 \cdot \mathbf{S}_2 + \mathbf{S}_2 \cdot \mathbf{S}_3) - 2\epsilon J_2 \mathbf{S}_1 \cdot \mathbf{S}_3\}$ on three sites from the Trotter decomposition of the partition function. By writing $\exp(-\epsilon J \mathbf{S}_i \cdot \mathbf{S}_j)$ as

$$\prod_{\alpha} \left[ \cosh(\epsilon J/4)\mathbb{1}_i \otimes \mathbb{1}_j - \sinh(\epsilon J/4)\sigma_i^{\alpha} \otimes \sigma_j^{\alpha} \right], \tag{14}$$

where $\alpha = x,y,z$, $\sigma^{\alpha}$ are Pauli matrices, and omitting higher orders of $O(\epsilon)$, one obtains

$$\begin{aligned} \hat{\mathbf{O}} = {} & \mathbb{1}_1 \otimes \mathbb{1}_2 \otimes \mathbb{1}_3 - \sum_{\alpha} \tanh(\epsilon J_1/4)\sigma_1^{\alpha} \otimes \sigma_2^{\alpha} \otimes \mathbb{1}_3 \\ & - \sum_{\alpha} \tanh(\epsilon J_1/4)\mathbb{1}_1 \otimes \sigma_2^{\alpha} \otimes \sigma_3^{\alpha} \\ & - \sum_{\alpha} \tanh(\epsilon J_2/2)\sigma_1^{\alpha} \otimes \mathbb{1}_2 \otimes \sigma_3^{\alpha}. \end{aligned} \tag{15}$$

The above terms can be expressed as a matrix product operator (MPO) [39],

$$\begin{aligned} \hat{\mathbf{O}} &= \sum_{i_1,i_2,i_3=0}^{3} \left(\mathbf{v}_{i_1}^T \mathbf{B}_{i_2} \mathbf{v}_{i_3}\right) \mathbf{X}_{i_1} \otimes \mathbf{X}_{i_2} \otimes \mathbf{X}_{i_3} \\ \mathbf{X}_0 &= \mathbb{1}, \quad \mathbf{X}_1 = \sigma^x, \quad \mathbf{X}_2 = \sigma^y, \quad \mathbf{X}_3 = \sigma^z, \\ \mathbf{v}_0 &= |0\rangle, \\ \mathbf{v}_i &= a|i\rangle \quad (i = 1,2,3), \\ \mathbf{B}_0 &= |0\rangle\langle 0| + b|1\rangle\langle 1| + b|2\rangle\langle 2| + b|3\rangle\langle 3|, \\ \mathbf{B}_i &= c|0\rangle\langle i| + c|i\rangle\langle 0| \quad (i = 1,2,3), \end{aligned} \tag{16}$$

where $\mathbf{v}_i$ are the vectors of length 4, $\mathbf{B}_i$ are 4×4 matrices, $\mathbf{X_i}$ are operators acting on the physical index, and $a,b,c$ are scalar variables. In order to correctly match the coefficients in front of each term in Eq. (15), $a,b,c$ have to be chosen to satisfy $ac = -\tanh(\epsilon J_1/4)$, $a^2 b = -\tanh(\epsilon J_2/2)$, and $|a|,|b|,|c| \ll 1$. Thus the evolution operators on these sites are written as $\hat{\mathbf{O}}_1 = \sum_i \mathbf{v}_i^T \otimes \mathbf{X}_i$, $\hat{\mathbf{O}}_2 = \sum_i \mathbf{B}_i \otimes \mathbf{X}_i$, and $\hat{\mathbf{O}}_3 = \sum_i \mathbf{v}_i \otimes \mathbf{X}_i$, respectively.

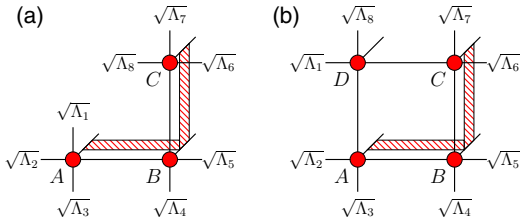


FIG. 7. (a) The simple update scheme. (b) The cluster update scheme with a cluster size 2×2.

We present the diagrammatic representation of the evolution operators $\hat{\mathbf{O}}_1$, $\hat{\mathbf{O}}_2$, and $\hat{\mathbf{O}}_3$ acting on sites $A$, $B$, and $C$ in a 2×2 cluster in Fig. 7(b). The corresponding simple update scheme is sketched in Fig. 7(a). In both cases, the complexity scales as $D^5$, and there is no cumulative error.

## ACKNOWLEDGMENTS

We would like to thank J. Richter for passing along their exact diagonalization data for comparison, F. Becca for passing along their variational Monte Carlo data for comparison, and A. W. Sandvik, Leon Balents, H.-C. Jiang, D. Sheng, S.-S. Gong, and Z.-Y. Zhu for their stimulating discussions. L.W. is supported by National Natural Science Foundation of China (NSFC-11474016), National Thousand Young Talents program of China. Z.C.G. is supported by startup support from Department of Physics, CUHK. F.V. is supported by the EU Strep Project QUEVADIS, the ERC Grant QUERG, and the FWF SFB Grants FoQuS and ViCoM. The computational results presented have been achieved partially using Tianhe-2JK computing time award at the Beijing Computational Science Research Center (CSRC).

[1] P. W. Anderson, The resonating valence bond state in $La_2CuO_4$ and superconductivity, Science **235**, 1196 (1987).
[2] For a review, see P. A. Lee, N. Nagaosa, and X. G. Wen, Doping a Mott insulator: Physics of high-temperature superconductivity, Rev. Mod. Phys. **78**, 17 (2006).
[3] V. Kalmeyer and R. B. Laughlin, Equivalence of the Resonating-Valence-Bond and Fractional Quantum Hall States, Phys. Rev. Lett. **59**, 2095 (1987).
[4] X.-G. Wen, F. Wilczek, and A. Zee, Chiral spin states and superconductivity, Phys. Rev. B **39**, 11413 (1989).
[5] N. Read and S. Sachdev, Large-$N$ Expansion for Frustrated Quantum Antiferromagnets, Phys. Rev. Lett. **66**, 1773 (1991).
[6] X.-G. Wen, Mean-field theory of spin-liquid states with finite energy gaps and topological order, Phys. Rev. B **44**, 2664 (1991).
[7] R. Moessner and S. L. Sondhi, Resonating Valence Bond Phase in the Triangular Lattice Quantum Dimer Model, Phys. Rev. Lett. **86**, 1881 (2001).
[8] H. Yao and S. A. Kivelson, Exact Spin-Liquid Ground States of the Quantum Dimer Model on the Square and Honeycomb Lattices, Phys. Rev. Lett. **108**, 247206 (2012).
[9] W.-J. Hu, F. Becca, A. Parola, and S. Sorella, Direct evidence for a gapless $Z_2$ spin liquid by frustrating Néel antiferromagnetism, Phys. Rev. B **88**, 060402(R) (2013).
[10] E. Dagotto and A. Moreo, Phase Diagram of the Frustrated Spin-1/2 Heisenberg Antiferromagnet in 2 Dimensions, Phys. Rev. Lett. **63**, 2148 (1989).
[11] F. Figueirido, A. Karlhede, S. Kivelson, S. Sondhi, M. Rocek, and D. S. Rokhsar, Exact diagonalization of finite frustrated spin-$\frac{1}{2}$ Heisenberg models, Phys. Rev. B **41**, 4619 (1990).

[12] H. J. Schulz and T. A. L. Ziman, Finite-size scaling for the two-dimensional frustrated quantum Heisenberg antiferromagnet, Europhys. Lett. **18**, 355 (1992).
[13] H. J. Schulz, T. A. L. Ziman, and D. Poilblanc, Magnetic order and disorder in the frustrated quantum Heisenberg antiferromagnet in two dimensions, J. Phys. I **6**, 675 (1996).
[14] T. Einarsson and H. J. Schulz, Direct calculation of the spin stiffness in the $J_1$-$J_2$ Heisenberg antiferromagnet, Phys. Rev. B **51**, 6151 (1995).
[15] J. Richter and J. Schulenburg, The spin-1/2 $J_1$-$J_2$ Heisenberg antiferromagnet on the square lattice: Exact diagonalization for $N = 40$ spins, Eur. Phys. J. B **73**, 117 (2010).
[16] P. Chandra and B. Doucot, Possible spin-liquid state at large $S$ for the frustrated square Heisenberg lattice, Phys. Rev. B **38**, 9335 (1988).
[17] N. E. Ivanov and P. Ch. Ivanov, Frustrated two-dimensional quantum Heisenberg antiferromagnet at low temperatures, Phys. Rev. B **46**, 8206 (1992).
[18] M. Arlego and W. Brenig, Plaquette order in the $J_1$-$J_2$-$J_3$ model: Series expansion analysis, Phys. Rev. B **78**, 224415 (2008).
[19] J. Sirker, Z. Weihong, O. P. Sushkov, and J. Oitmaa, $J_1$-$J_2$ model: First-order phase transition versus deconfinement of spinons, Phys. Rev. B **73**, 184420 (2006).
[20] R. Darradi, O. Derzhko, R. Zinke, J. Schulenburg, S. E. Krüger, and J. Richter, Ground state phases of the spin-$\frac{1}{2}$ $J_1$-$J_2$ Heisenberg antiferromagnet on the square lattice: A high-order coupled cluster treatment, Phys. Rev. B **78**, 214415 (2008).
[21] K. S. D. Beach, Master equation approach to computing RVB bond amplitudes, Phys. Rev. B **79**, 224431 (2009).
[22] M. Mambrini, A. Läuchli, D. Poilblanc, and F. Mila, Plaquette valence-bond crystal in the frustrated Heisenberg quantum antiferromagnet on the square lattice, Phys. Rev. B **74**, 144422 (2006).
[23] L. Capriotti, F. Becca, A. Parola, and S. Sorella, Resonating Valence Bond Wave Functions for Strongly Frustrated Spin Systems, Phys. Rev. Lett. **87**, 097201 (2001).
[24] L. Capriotti and S. Sorella, Spontaneous Plaquette Dimerization in the $J_1$-$J_2$ Heisenberg Model, Phys. Rev. Lett. **84**, 3173 (2000).
[25] H.-C. Jiang, H. Yao, and L. Balents, Spin-liquid ground state of the spin-$\frac{1}{2}$ square $J_1$-$J_2$ Heisenberg model, Phys. Rev. B **86**, 024424 (2012).
[26] S.-S. Gong, W. Zhu, D. N. Sheng, O. I. Motrunich, and M. P. A. Fisher, Plaquette Ordered Phase and Quantum Phase Diagram in the Spin-$\frac{1}{2}$ $J_1$-$J_2$ Square Heisenberg Model, Phys. Rev. Lett. **113**, 027201 (2014).
[27] F. Verstraete and J. I. Cirac, Renormalization algorithms for quantum-many body systems in two and higher dimensions, arXiv:cond-mat/0407066.
[28] L. Wang and F. Verstraete, Cluster update for tensor network states, arXiv:1110.4362.
[29] L. Wang, D. Poilblanc, Z.-C. Gu, X.-G. Wen, and F. Verstraete, Constructing Gapless Spin-Liquid State for the Spin-$\frac{1}{2}$ $J_1$-$J_2$ Heisenberg Model on a Square Lattice, Phys. Rev. Lett. **111**, 037202 (2013).
[30] A. W. Sandvik, Evidence for Deconfined Quantum Criticality in a Two-Dimensional Heisenberg Model with Four-Spin Interactions, Phys. Rev. Lett. **98**, 227202 (2007).
[31] A. W. Sandvik, Continuous Quantum Phase Transition between an Antiferromagnet and a Valence-Bond Solid in Two Dimensions: Evidence for Logarithmic Corrections to Scaling, Phys. Rev. Lett. **104**, 177201 (2010).
[32] H. Shao, W. Guo, and A. W. Sandvik, Quantum criticality with two length scales, Science **352**, 213 (2016).
[33] T. Senthil, A. Vishwanath, L. Balents, S. Sachdev, and M. Fisher, Deconfined quantum critical points, Science **303**, 1490 (2004).
[34] T. Senthil, L. Balents, S. Sachdev, A. Vishwanath, and M. P. A. Fisher, Quantum criticality beyond the Landau-Ginzburg-Wilson paradigm, Phys. Rev. B **70**, 144407 (2004).
[35] L. Wang, I. Pižorn, and F. Verstraete, Monte Carlo simulation with tensor network states, Phys. Rev. B **83**, 134421 (2011).
[36] M. Levin and C. P. Nave, Tensor Renormalization Group Approach to 2D Classical Lattice Models, Phys. Rev. Lett. **99**, 120601 (2007).
[37] Z.-C. Gu, M. Levin, and X.-G. Wen, Tensor-entanglement renormalization group approach as a unified method for symmetry breaking and topological phase transitions, Phys. Rev. B **78**, 205116 (2008).
[38] V. Murg, F. Verstraete, and J. I. Cirac, Exploring frustrated spin systems using projected entangled pair states, Phys. Rev. B **79**, 195119 (2009).
[39] B. Pirvu, V. Murg, J. I. Cirac, and F. Verstraete, Matrix product operator representations, New J. Phys. **12**, 025012 (2010).